Combined X-ray Diffraction and QM/MM Study of the *Burkholderia cepacia* Lipase-Catalyzed Secondary Alcohol Esterification

Marija Luić,*,† Zoran Štefanić,† Igor Ceilinger,‡ Milan Hodošček,§ Dušanka Janežič,§ Tihana Lenac,|| Ivana Leščić Ašler,† Dragan Šepac,⊥ and Sanja Tomić*,†

Rudjer Bošković Institute, Bijenička 54, HR-10000 Zagreb, Croatia, Belupo d.d., Danica 5, HR-48000 Koprivnica, Croatia, National Institute of Chemistry, Hajdrihova 19, SI-1000 Ljubljana, Slovenia, Faculty of Medicine, Braće Branchetta 20, HR-51000 Rijeka, Croatia, and Pliva-Research and Development Ltd., Prilaz baruna Filipovića 29, HR-10000 Zagreb, Croatia

Received: September 26, 2007; In Final Form: January 31, 2008

To understand the origin of high enantioselectivity of *Burkholderia cepacia* lipase (BCL) toward secondary alcohol, (*R*,*S*)-1-phenoxy-2-hydroxybutane (**1**), and its ester (**E1**), we determined the crystal structure of BCL complexed with phosphonate analogue of *S*-**E1** and accomplished a series of MM, MC, and QM/MM studies. We have found that the inhibitor in the *S* configuration binds into the BCL active site in the same manner as the *R* isomer, with an important difference: while in case of the *R*-inhibitor the H-bond between its alcohol oxygen and catalytic His286 can be formed, in the case of the *S*-inhibitor this is not possible. Molecular modeling for both **E1** enantiomers revealed orientations in which all hydrogen bonds characteristic of productive binding are formed. To check the possibility of chemical transformation, four different orientations of the substrate (two for each enantiomer) were chosen, and a series of ab initio QM/MM calculations were accomplished. Starting from the covalent complex, we modeled the ester (**E1**) hydrolysis and the alcohol (**1**) esterification. The calculations revealed that ester release is possible starting with all four covalent complexes. Alcohol release from the BCL−**E1** complex in which the *S*-substrate is bound in the same manner as the *S*-inhibitor in the crystal structure however is not possible. These results show that the crystallographically determined binding modes should be taken with caution when modeling chemical reactions.

Introduction

Lipases (triacylglycerol acylhydrolase, E.C. 3.1.1.3) are ubiquitous enzymes that hydrolyze ester bonds of triacylglycerols. However, their substrate specificity is not limited to triacylglycerols. In contrast to most other enzymes, they accept a wide range of unnatural substrates[1−5] and are stable in organic solvents. Many lipases also show high enantioselectivity toward chemically and pharmaceutically important compounds in addition to being environmentally friendly. Especially important for industrial use are lipases from microorganisms, which are often commercially available. They offer a more efficient route to enantiomerically pure products than do standard chemical methods.

One of the most frequently used is a lipase from bacteria *Burkholderia cepacia* (BCL, formerly called *Pseudomonas cepacia* lipase). This enzyme catalyzes esterification of both primary and secondary alcohols with good enantioselectivity producing compounds, which are important building blocks for many chiral drugs. The crystal structures of the native BCL and its complexes with triglyceride-like inhibitors were solved by 1998,[6−9] and, with numerous kinetic measurements available for this enzyme, this encouraged molecular modeling studies.[10−17] However, the mechanism of BCL catalysis and the basis of its enantioselectivity are still not completely understood.

Studying the lipase-catalyzed kinetic resolution of a series of secondary alcohols, Ljubović and Šunjić[18] found that among 30 commercially available lipases the *Burkholderia cepacia* lipase was the most efficient in resolution of racemic 1-phenoxy-2-hydroxybutane (**1**) (enantiomeric ratio $E \geq 200$), with the *R*-enantiomer being the fast-reacting one. Lipase-catalyzed ester hydrolysis (Scheme 1a) involves two successive tetrahedral intermediates. The first tetrahedral intermediate TI releases the alcohol and forms the acyl enzyme (Scheme 1b), while the second tetrahedral intermediate releases the acid. Only TI includes alcohol moiety and therefore contributes to the enantioselectivity of lipases toward chiral alcohols. TI is characterized by five hydrogen bonds. To study the mechanism of this reaction, it is necessary to know the orientation of a substrate in the BCL active site. The orientations used in this study were either derived by molecular modeling or determined by X-ray crystallography. The TI formed in the lipase-catalyzed reactions is unstable, and enzyme−inhibitor complexes, the crystal structures of which are available, are often used to approximate it. In our previous work, we solved the crystal structure of the BCL-secondary alcohol-like inhibitor complex (*R*-complex), in which a phosphonate inhibitor of the lipase (*R*-inhibitor) mimics the fast-reacting enantiomer. The *R*-inhibitor in this complex is bound in the active site with an orientation that enables formation of the five aforementioned H-bonds (Scheme 1b) and is similar to the one predicted by molecular modeling studies.[14,15]

In this work, we present the crystal structure of the BCL complexed with the phosphonate inhibitor (*S*-inhibitor) mimick-

* Corresponding author. E-mail: marija.luic@irb.hr (M.L.), sanja.tomic@irb.hr (S.T.).
† Rudjer Bošković Institute.
‡ Belupo d.d.
§ National Institute of Chemistry.
|| Faculty of Medicine.
⊥ Pliva-Research and Development Ltd.

10.1021/jp077717u CCC: $40.75 © 2008 American Chemical Society
Published on Web 04/03/2008

SCHEME 1: Phosphonates Mimic the Tetrahedral Intermediate in the BCL-Catalyzed Resolution of E1[a]

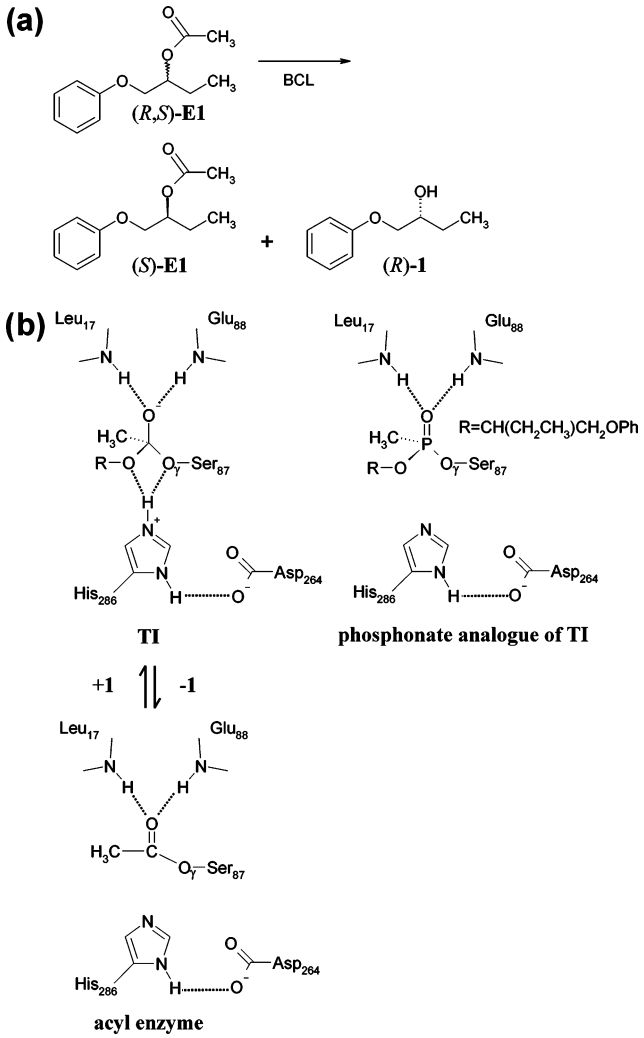

[a] (a) BCL-catalyzed hydrolysis of racemic **E1** yields *S*-**E1** and *R*-**1**. (b) The first tetrahedral intermediate TI releases alcohol (ROH) to form an acyl enzyme in the BCL-catalyzed hydrolysis of esters. The phosphonate analogue mimics TI. **1** denotes 1-phenoxy-2-hydroxybutane, and **E1** denotes its ester, 1-phenoxy-2-acetoxybutane.

ing the slow-reacting enantiomer, and the results of QM/MM study of the BCL-catalyzed transformations of both fast- and slow-reacting enantiomers of **1**. The *S*-inhibitor is bound into the BCL active site in the same orientation as the *R*-inhibitor but without the possibility to form a hydrogen bond with catalytic histidine (His286); see Scheme 1b. Inhibitor (phosphonate analogue of the secondary alcohol ester, **E1**) binds covalently to Ser87 by releasing chlorine,[19] and we speculate that simultaneously to this reaction the hydrogen from Ser87 is also released. However, reaction of substrate binding, either ester or alcohol, is different. Binding of the ester to Ser87 occurs simultaneously with the proton transfer from Ser87 to His286, while the alcohol binding to acylated Ser87 occurs spontaneously with the proton transfer from alcohol oxygen to Nϵ2 of His286. In the BCL−**E1** complex, His286 is positively charged (both nitrogen atoms of imidazole ring have an H attached), and in the BCL−inhibitor complex it is neutral. To elucidate the possibilities for the chemical transformation of **1** bound in different orientations and to track differences in the reactions of two enantiomers, a series of QM/MM calculations were carried out.

Experimental Protocols

Protein, Inhibitor, and Protein−Inhibitor Complex Preparation. *Lipase Preparation.* A commercial preparation of *B. cepacia* lipase (LPS AW 02513) was obtained from Amano Pharmaceuticals, Co., Nagoya, Japan. Because the preparation obtained contained large amounts of various impurities, it was further purified as described previously.[19] The final lipase preparation was concentrated to 17 mg mL^{-1} in 1 mM phosphate buffer pH 7.

Preparation of the Inhibitor (R_p,S_p)-O-(2S)-(1-phenoxybut-2-yl)-methyl-phosphonic Acid Chloride. The inhibitor was prepared starting from the enantiomerically pure secondary alcohol, (*S*)-1-phenoxy-2-hydroxybutane, following the procedure described previously.[19] The methylphosphonium dichloride $CH_3P(O)Cl_2$ was used as the phosphorus-acylating agent to introduce the $CH_3P(O)-O$ group, which mimics configuration and charge distribution of the tetrahedral intermediate $CH_3C-(O)-O$ group (see Scheme 1b). *Caution:* Methylphosphonium dichloride $CH_3P(O)Cl_2$ is highly toxic and must be handled with extreme caution.

Complex Preparation. Because of its high instability in air and water, freshly prepared (R_pS_p)-*O*-(2*S*)-(1-phenoxybut-2-yl)-methyl-phosphonic acid chloride was dissolved under argon in acetonitrile and added to the lipase solution (17 mg mL^{-1} in 1 mM Na phosphate pH 7) in molar ratios of 60:1, 40:1, and 20:1. By leaving chlorine covalently bound, lipase−inhibitor complex was formed.

Crystallization, X-ray Data Collection, and Refinement. The complex was crystallized by the hanging drop vapor diffusion technique at 18 °C using VDX plates and siliconized glass cover slips. The droplet was prepared by mixing 1 μL of complex solution with 1 μL of precipitant solution and equilibrated against 0.7 mL of reservoir solution. The reservoir solutions consisted of 25−55% (v/v) 2-propanol in 100 mM Tris/HCl, pH 8.5 and 40−44% (v/v) 2-methyl-2,4-pentanediol (MPD), 100 mM sodium citrate in 100 mM Hepes, pH 7.5. Similar conditions were used for the native protein crystallization[7] and for the BCL complexed with the same inhibitor, but a different enantiomer.[19] After several days, crystals appeared in both the 2-propanol and the MPD solution.

A crystal grown from 40% MPD, 100 mM sodium citrate, and 100 mM Hepes 7.5 was used for data collection. A complete X-ray dataset to 1.8 Å was collected at 100 K using a MAR research 345 mm image plate detector mounted on a Rigaku RU-H2R rotating anode X-ray generator (50 kV, 92 mA, 3 × 0.3 mm^2 focus, Xenox mirrors, Cu Kα radiation). Data were processed using the HKL2000 program,[20] and the intensities were converted to structure-factor amplitudes using the program TRUNCATE[21] from the CCP4[22] suite of crystallographic programs. The data collection and refinement statistics are summarized in Table 1. The lipase−inhibitor complex crystallized in the monoclinic space group *C*2 with unit cell parameters $a = 89.01$ Å, $b = 46.58$ Å, $c = 84.24$ Å, $\beta = 121.01°$, and one molecule in the asymmetric unit ($Z = 4$).

As expected, the crystal structure of the *S*-complex is isomorphous to the *R*-complex (PDB code 1HQD) structure whose atomic coordinates were used directly in refinement with the CNS program.[23] Omit and difference electron density maps ($2F_o - F_c$ and $F_o - F_c$) were calculated with the same program. Model building and map inspections were performed using the O program.[24] Initial Fourier maps $2F_o - F_c$ and $F_o - F_c$ showed prominent electron density features in the active site region, revealing that the inhibitor molecule is covalently bound to the Oγ of the catalytic residue Ser87. A model for the inhibitor

TABLE 1: Crystal Cell Parameters, Data Collection, and Refinement Statistics for the *Burkholderia cepacia* Lipase Complexed with the *S*-Inhibitor

Crystal Cell Parameters	
space group	*C*2
unit cell parameters (Å, deg)	$a = 89.01$, $b = 46.58$, $c = 84.24$, $\beta = 121.0$
Data Collection Statistics (23.6−1.8 Å)	
temp (K)	100
total reflections	98 256
unique reflections	27 385 (2339)[a]
completeness (%)	97.5 (84.3)
R_{sym}[b]	0.058 (0.27)
mean $I/\sigma(I)$	31.1 (4.8)
Refinement Statistics	
R-factor	0.175
R_{free}	0.213
rms Deviation from Ideal Geometry	
bond lengths (Å)	0.005
bond angles (deg)	1.3
number of protein atoms	2338
number of inhibitor atoms	15
number of metals	2
number of waters	302
average *B* factor	20.23

[a] Values in parentheses refer to the highest resolution shell (1.8−1.85 Å). [b] $R_{sym} = \sum_{hkl}|I_{hkl} - \langle I\rangle|/\sum_{hkl}I_{hkl}$ (single measurements excluded).

was built and introduced into the atomic coordinates set for further refinement after an initial refinement limited to the enzyme molecule. As in the case of *R*-complex, after locating the oxygen bound to phosphorus into the oxyanion hole, only the S_p enantiomer could be fitted into the positive electron density of the Fourier map. Similarly as in one of the three available models (PDB code 3LIP) for the native protein as well as in *R*-complex (PDB code 1HQD), the peptide bond Gln292−Leu293 near the calcium-binding site adopts a cis conformation.

The final model includes all 320 amino acids, one inhibitor molecule, one Ca^{2+} ion, one metal atom assumed to be Na^+, and 302 water molecules with good hydrogen-bonding geometry (Ow···O/N distances in the range of 2.3−3.5 Å). The correctness of stereochemistry was finally checked using PROCHECK.[25] The refinement was performed without σ cutoff giving the final crystallographic *R* value of 17.5% and R_{free} 21.3%. Coordinates and structure factors have been deposited with the Protein Data Bank (accession code 2NW6).

QM/MM Calculations. Molecular modeling was performed starting from the crystal structures of the complex of BCL with the phosphonate analogues, *R* and *S*, of 1-phenoxy-2-acetoxybutane, **E1** (ester of 1-phenoxy-2-hydroxybutane, **1**), Protein Data Bank codes 1HQD[19] and 2NW6, respectively. The $P(CH_3)O^-$ group covalently bound to Ser87 was replaced by the $C(CH_3)O^-$ group, and in this way the so-called crystallographic binding modes of 1-phenoxy-2-hydroxybutane, **Rc** and **Sc**, were determined. The **Rm** and **Sm** binding modes were determined by the Monte Carlo Multiple Minimum (MCMM) and low mode conformational searches as described previously.[15,26] The complexes were solvated in the 7 Å thick TIP3P water layer and energy minimized without constraints by CHARMM[27] using the all-atom force field CHARMM22.[28] All aspartic and glutamic acids were negatively charged, and arginines and lysines were positively charged. Histidines were uncharged, except the catalytic His286, which was positively charged (both nitrogen atoms of the imidazole ring have an H attached).

The esterification and hydrolysis reactions were modeled starting from the four geometry-optimized hydrated complexes of BCL−(*R*,*S*)-**E1**, two for each enantiomer, which for simplicity are named **Rc**, **Rm**, **Sc**, and **Sm**. Separation into QM and MM segments was the same in all of the complexes with the border distant from the atoms that undergo hybridization change during the course of the reaction. Parts of the complex that are chemically transformed in the reactions, the substrate and the side chains of His286 and Ser87, were treated quantum mechanically, and the remainder of the protein and water were treated classically. Because the border between QM and MM region bisects two covalent bonds, Cα−Cβ of His286 and Ser87, we introduced two link atoms to saturate the open valence atoms in QM region. The link atoms were treated as hydrogens, and their positions were minimized along the other parameters. Including the link atoms, the QM region comprised 51 atoms, and the MM part more than 10 000 atoms (10 154 in the final structures with identical MM segment). The QM part was treated by the density functional method (GAMESS-US[29]) at the B3LYP/6-31G(d) level of theory, and the MM part by the CHARMM22 force field.[28] The interaction between these two regions is described by QM/MM Hamiltonian, $H_{QM/MM} = H_{bonded} + H_{vdw} + H_{elec}$. The bonded and van der Waals interactions were treated classically as described earlier,[30] and electrostatic interactions were evaluated from the QM electrostatic potential and the MM partial charges in a way that the MM atoms were treated as external charges interacting with QM atoms through the one-electron integrals. No cutoffs were introduced for the nonbonding MM and QM/MM interactions.

After the initial structures (IS) were QM/MM geometry optimized with 10 000 adopted basis Newton−Raphson (ABNR) steps, hydrogen from the protonated His286 was moved either in the direction of the serine Oγ oxygen or toward the substrate alcohol oxygen, using the restrained distance (RESD) method. In this method, the reaction coordinate is followed by placing large restraints (force constant was set to 1000 kcal mol^{-1} $Å^{-2}$) on the degrees of freedom most critical to the proposed mechanism. The increment utilized for the proton transfer was 0.1 Å, and after each movement, the energy was optimized using the ABNR method for 100 steps. In this way, the minimum energy pathways for the alcohol, **1**, esterification and its ester, **E1**, hydrolysis were determined.

Because the initial conformations of the proteins (from 1HQD and 2NW6, both optimized) differ slightly (rms distance 0.13 Å), we inserted in the last stage of our study the key substrate structures from the reaction paths: initial state (IS), products (P1 − ester, P2 − alcohol), and transition states (TS1 and TS2) into the same protein (**Sc**), reoptimized complexes (using restraints), and recalculated their energies without restraints, Table 2.

TABLE 2: The Relative Energies Calculated for Different Covalent Complexes, TIs, between Acyl-BCL and *R*-1 and *S*-1[a]

	E/kcal mol^{-1}	
	no water	water
Rc	3.5	0.0
Rm	0.0	1.3
Sc	*8.7*	*5.7*
Sm	9.0	8.8

[a] The energies for **Sc** are given in italic because, according to our calculations, the secondary alcohol ester bound in this orientation cannot be hydrolyzed.

Results and Discussion

Crystallographic Studies. Crystals of the complex formed by the lipase and the *S*-inhibitor were isomorphous with those

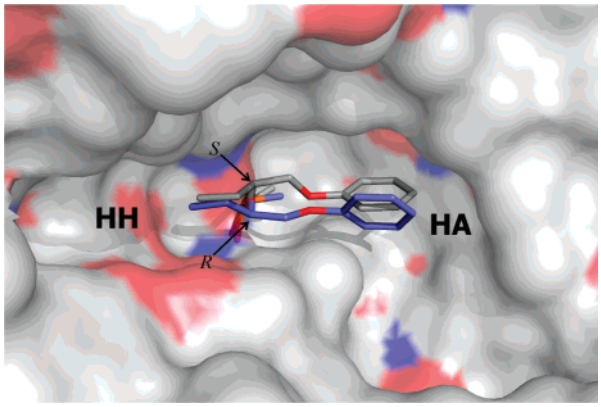

Figure 1. Mirror-image packing of the superimposed *R*- and *S*-complexes in the BCL active site.

of the native protein[6,7] (PDB codes 1OIL, 2LIP, and 3LIP) as well as complexed[8,19] (5LIP and 1HQD), and this allowed for the determination of the crystallographic structure by difference Fourier techniques. The model (1HQD without inhibitor and water molecules) was refined using the CNS program[23] to crystallographic *R*-factor and R_{free} values of 0.175 and 0.213, respectively. The Ramachandran plot shows that Leu234 lies in a disallowed region, as has been already observed for the native protein.[7] An rms deviation value of 0.351 Å was calculated over all Cα atoms with respect to the unbound enzyme (3LIP). With respect to the *R*-complex, the rms value is 0.130 Å. The statistics for data collection and refinement are summarized in Table 1.

The *S*-inhibitor binds to BCL in the same way as the *R*-inhibitor. Both covalently link the phosphorus to the catalytic Ser87 Oγ atom and have S_P configuration. Nucleophilic attack at phosphorus by Ser87 Oγ likely proceeds with inversion of configuration at phosphorus.[31] In view of the fact that as a result of this reaction the priorities of the substituents at the phosphorus change as well (defined by rules of Cahn, Ingold, and Prelog),[32] the *S*-inhibitor had S_p configuration prior to the reaction. The chiral carbon atoms differ in positions by 1.16 Å (Figure 1).

From Figures 1 and 2, it is clear that three substituents on the chiral carbon atom lie in a similar position in both structures. If we define binding pockets in accordance with Lang and co-workers,[8] examination of the active site with Ser87 at the bottom and His286 situated above the substrate reveals that the large hydrophobic pocket HA is on the right side of His286, the mixed hydrophobic−hydrophilic HH pocket is on the left, and HB lies between them. The large phenoxy group on the chiral carbon is accommodated in HA pocket, and the medium-sized alkyl group points toward HH. When three substituents are similarly located, the fourth substituent (hydrogen) must point in the opposite direction. In this way, the two enantiomers adopt orientations that are mirror images of one another. By analysis of the X-ray crystal structures of enantiomeric ligands bound to enzymes, Mezzetti et al.[33] found that such mirror-image packing is a common orientation. Surprisingly, although this mirror-image packing has been proposed as early as in 1981,[34] most researchers had treated the orientation of enantiomers in the enzyme active site only through exchange of the positions of two substituents.[33]

As in all serine hydrolases, the reactive center in BCL is composed of an oxyanion cavity, bounded by Leu17 and Gln88, and a catalytic triad formed by Ser87, His286, and Asp264. Serine functions as the nucleophile, histidine plays a dual role as proton acceptor or proton donor, but the role of Asp and the precise nature of the histidine−aspartate interaction are still unclear.

The oxyanion cavity is occupied by a phosphoryl oxygen atom (O1), which forms H-bonds to the peptide N−H groups of Leu17 and Gln88 (Figure 2 and Table 3).

The Ser87 Oγ atom is at a hydrogen-bond distance from the side-chain nitrogen of His286 Nϵ2, but the alcohol oxygen O2 is 3.71 Å apart from it, and differently from the *R*-complex structure the O2···Nϵ2 hydrogen bond is not possible. If we add hydrogen atoms to this model, we can see that the hydrogen at His286 Nϵ2 is only 1.97 Å from the hydrogen at the alcohol stereocenter (*C2*), suggesting that His286 does not have hydrogen bound to Nϵ2. The covalent bond formation between the substrate, either alcohol or its ester, and the catalytic serine (Ser87) is accompanied by a hydrogen atom binding to Nϵ2 of His286; that is, H from either the secondary alcohol or the Ser87 (in the case of ester binding) moves toward His286 and binds to Nϵ2. However, covalent binding of the inhibitor to Ser87 proceeds differently. Upon binding of the inhibitor the Cl ion is released, it very probably attracts the hydrogen from Ser87, and they together leave the lipase active site. According to this assumption, His286 is neutral in the BCL−inhibitor complex; that is, there is no H bound to its Nϵ2. As mentioned above, the five hydrogen bonds displayed at Scheme 1b are considered necessary for productive binding of a substrate, that is, for the reaction to occur. This suggests that the crystal structure of the *S*-complex, which does not mimic a catalytically productive binding of the substrate, is not a good model for the tetrahedral intermediate for the slow-reacting enantiomer.

Although the general mechanism of lipase catalysis is established, the precise detail of catalytic serine activation is still a subject of debate. Derewenda et al.[36] found that in various serine hydrolases, the Cϵ of the active site histidine is in a close contact with the main-chain carbonyl oxygen. They proposed that the His286 Cϵ1−H···O═C< bond affects the charge distribution within the imidazolium ion. In the native BCL structure (PDB code 3LIP) as well as in BCL complexed with both our enantiomeric phosphonate inhibitors (PDB codes 1HQD and 2NW6), the catalytic His286 Cϵ1−H···O═C< Gly111 distance is slightly over 3.3 Å, which corresponds to their sum of the van der Waals radii (3.32 in 3LIP, 3.39 in 1HQD, and 3.32 Å in 2NW6); that is, the Cϵ1−H···O═C hydrogen bond does not exist. In 1997, Cassidy et al.[37] proposed a new concept for the mechanism of action of serine proteases, postulating the formation of a low barrier hydrogen bond (LBHB) in the catalytic dyad His−Asp, suggesting that it enhances the reactivity of catalytic serine by increasing the positivity of the catalytic histidine and thus facilitating the formation of a tetrahedral intermediate. Kuhn et al.[38] designated the same H-bond as a catalytic hydrogen bond, CHB, and not LBHB in which the hydrogen is located in between donor and acceptor. In their case, hydrogen is 1.2 Å from the His Nδ1 and 1.5 Å from the Asp Oδ2. Comparing the His−Asp distances in free BCL structures (PDB codes 1OIL, 2LIP, and 3LIP) to the BCL complexed structures (PDB codes 4LIP, 5LIP, 1HQD, and 2NW6) reported to date, no shortening of this distance in complexed structures was observed, suggesting that this is neither an LBHB nor a CHB.

Molecular Modeling

To understand the process of BCL-catalyzed esterification of the racemate (±)-1-phenoxy-2-hydroxybutane and to investigate if the reaction is possible for the slow-reacting substrate

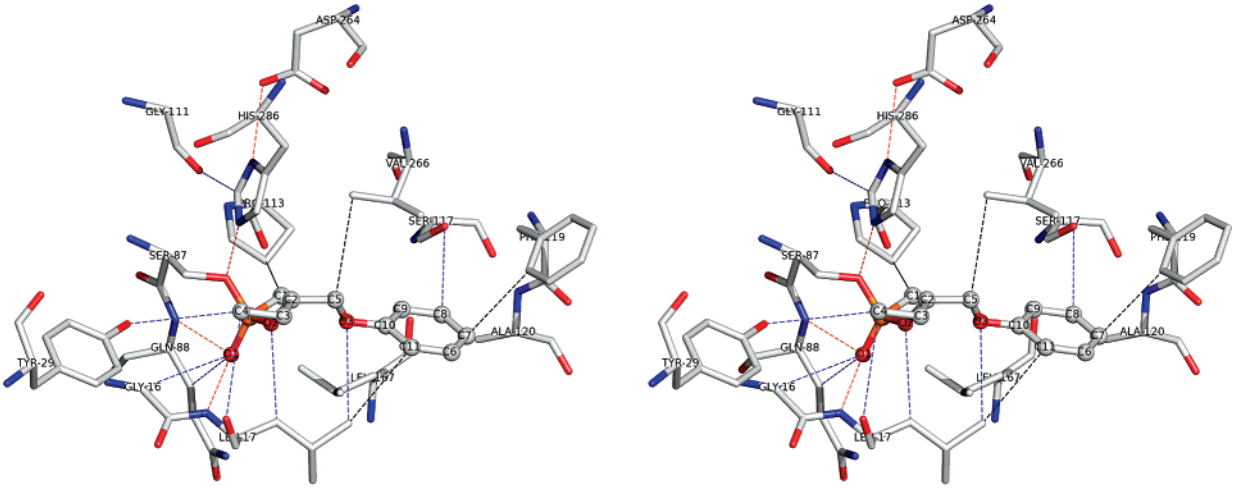

Figure 2. The view at the BCL active site containing the bound *S*-inhibitor with interactions described in Table 2. The possible H-bonds are shown in red, nonpolar contacts in black, and C(H)−O distances in blue.

TABLE 3: Distances between Atoms Involved in Formation of H-Bonds in TI and Inhibitor−Enzyme Interactions below 4 Å Detected in *R*- and *S*-Complexes

Possible Hydrogen Bonds		
	distance (Å)	
	R	*S*
Leu17 N···O1=P	2.73	2.67
Gln88 N···O1=P	2.99	2.76
His286 Nϵ2···Oγ Ser87	2.94	2.84
His286 Nδ1···Oδ2	3.18	2.82
His286 Nϵ2···O2	3.23	

Interactions (<4 Å)		
	distance (Å)	
nonpolar interactions	*R*	*S*
Phe119 Cδ2···Phe[a]	3.64	3.40
Leu167 Cδ1···Phe	3.61	4.17
Leu17 Cδ2···Phe	3.81	3.46
Leu167 Cδ1···C1	3.65	4.20
Leu167 Cδ2···C1	3.94	4.34
Val266 Cγ2···C5	5.02	3.73
Pro113 Cγ···C1	4.07	3.97
	distance (Å)	
C−(H)···O interactions	*R*	*S*
Leu17 Cδ2···O3	3.73	3.53
C2···O=C Leu17	3.46	4.87
Val266 Cγ1···O3	3.84	4.42
Tyr29 OH···C4	3.55	3.99
C3···O=C Leu17	3.59	4.08
C4···O=C Leu17	3.55	3.80
Gln88 Cβ1···O1	2.99	2.90
Leu17 Cβ···O2	4.62	3.44
His286 Cϵ···O=C Gly111	3.39	3.32
C8···O=C Ser117	5.62	3.68
Gly16 Cα···O1	3.38	3.55

[a] Shortest distance to the phenyl ring of the inhibitor.

bound in the same orientation as its phosphonate analogue in the crystal structure 2NW6, we accomplished a series of QM/MM calculations. In contrast to the behavior of the fast-reacting enantiomer, the orientation predicted by the molecular modeling[14,15] of the slow-reacting enantiomer in the BCL active site differs from that determined experimentally.

Starting from four different initial structures, two for each enantiomer of 1-phenoxy-2-hydroxybutane (**1**), we modeled ester hydrolysis and alcohol esterification (Scheme 2). **Rc** and **Sc** represent crystal structures, and **Rm** and **Sm** are the modeled

SCHEME 2: Reactions Studied by the QM/MM Method[a]

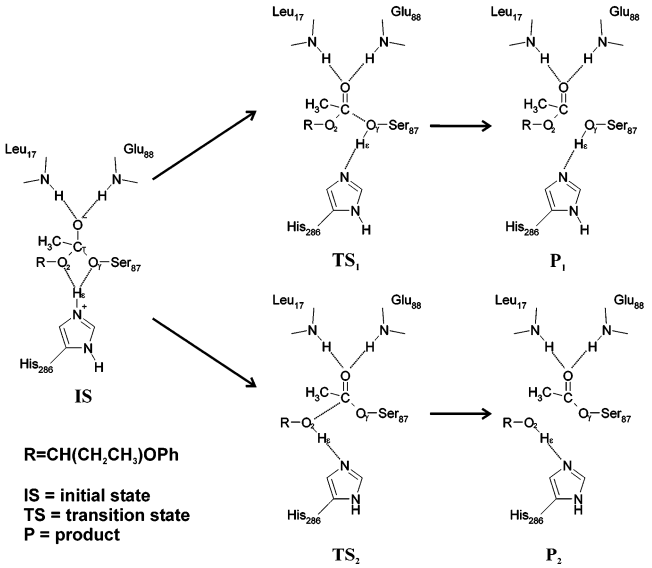

[a] IS is the initial structure, P1 and P2 are results of esterification and hydrolysis, respectively, while TS1 and TS2 are transition points for these reactions.

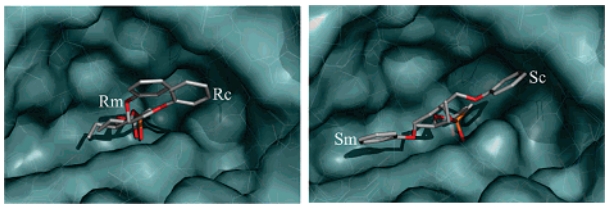

Figure 3. The four initial structures used in QM/MM calculations: (a) overlap of the two BCL−*R*-**E1** complexes **Rc** and **Rm**, and (b) overlap of the two BCL−*S*-**E1** complexes **Sc** and **Sm**.

structures. **Rc** and **Rm** stand for BCL−*R*-**E1** complexes, and **Sc** and **Sm** stand for BCL−*S*-**E1** complexes (Figure 3).

All of the relevant H-bonds are present in **Rc** (Scheme 1b), but in **Sc** the H-bond between His286 (Hϵ) and the O of the alcohol is missing, and according to our earlier quantum mechanical calculations,[26] performed on the reduced systems, hydrolysis cannot be accomplished starting from this structure. Our previous molecular modeling study[15] revealed several orientations with five characteristic hydrogen bonds (Scheme 1b) for the fast-reacting enantiomer in the BCL active site, but

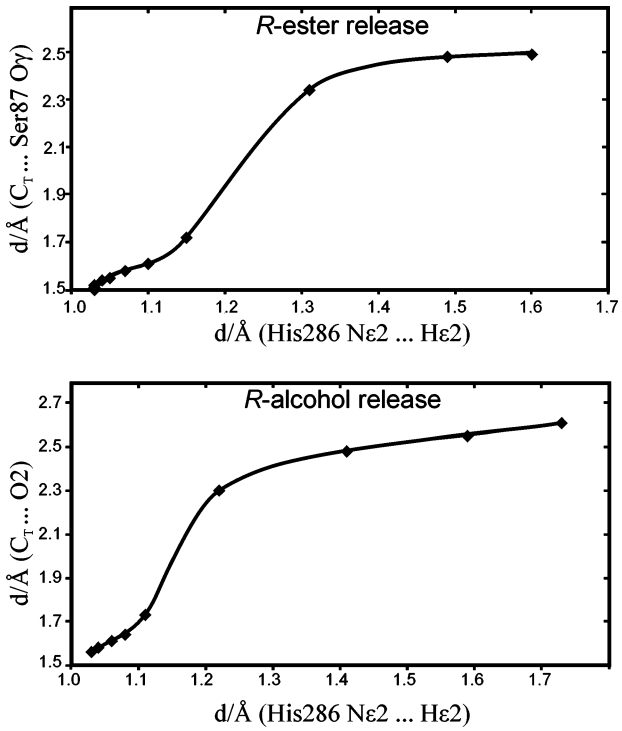

Figure 4. Minimum energy reaction paths depicted in the 2D-reaction coordinate diagrams for the ester release (top) and for the alcohol release (bottom) starting from the **Rc** binding mode.

only one orientation for the slow-reacting enantiomer. This orientation differs significantly from that found for the inhibitor in the crystal structure (Figures 1 and 3). Instead of adopting a binding in the mirror-image orientation similar to the *R*-enantiomer (with the phenyl ring accommodated in the large, hydrophobic HA pocket), the binding of the *S*-enantiomer is predicted by molecular modeling to be in the opposite orientation (that is, with phenyl ring accommodated in the partly hydrophilic HH pocket) (Figure 3). This could be explained by the fact that in the search for possible orientations only structures resembling the tetrahedral intermediate geometry were considered; details of the procedure used can be found in our previous work.[15] For the present study, we have chosen the lowest energy orientations named **Rm** and **Sm**, shown in Figure 3.

Initial complexes were hydrated, and after QM/MM optimization the reactions of hydrolysis and esterification were modeled in a way that the His286 Hϵ2 moved to either the alcohol oxygen (O2) or the serine Oγ. As proposed by Anderson et al.,[39] the process of ester release modeled in this work is accompanied by a decrease in the electron density of the nucleophile, Oγ of Ser87. In IS, the electronegativity of Oγ is decreased by the hydrogen bond to the protonated His286. As the reaction proceeds, the Hϵ2 moves from His286 to Oγ of Ser87, facilitating breaking of the C_T–Oγ covalent bond (Figure 4). Similarly, in the ester hydrolysis reaction, the nucleophilicity of the alcohol oxygen is decreased by hydrogen bonding to the protonated His286. A further decrease in nucleophilicity results from the movement of Hϵ2 toward the alcohol oxygen.

The minimum energy reaction paths, connecting the covalent complex (IS) with noncovalent complexes between BCL and the substrate, ester (P1) and alcohol (P2), are shown in the 2D-reaction coordinate diagrams for the **Rc** binding mode (Figure 4). It is interesting that a small change in the position of Hϵ2 induces breaking of the covalent bond.

In **Sc**, the proton transfer to alcohol does not occur. The hydrogen spontaneously turns toward Ser87, an energetically more favorable direction, and the approach of the hydrogen to Oγ leads to breaking of the C−Oγ bond. Similar results were obtained with the quantum mechanical, transition point searching calculations carried out on the reduced system consisting of 22 amino acids that include the BCL active site and the substrate.[26] The relative energies of the key points at the energy profiles, P1, P2, transition points (TS1 and TS2), and initial state (IS) (see Scheme 2), are given in Table 4. Contrary to the crystal structures (PDB codes 1HQD and 2NW6) in all of the initial complexes (IS), a weak hydrogen bond Cϵ1−H···O=C< between the catalytic His286 and Gly111 is formed. During optimization (after hydrogen atoms adding) of the crystal structures, the Cϵ1···O=C< distance drops below 3.0 Å (see Table 3 for reference). The H···O distance is 1.90 Å in the modeled complexes and 2.01 and 1.84 Å in the optimized **Rc** and **Sc** complexes, respectively. The strength of the hydrogen bond does not change in TS1 (see Scheme 2), the transition state in the ester release reaction, but is weaker in TS2 (H···O distance >2.10 Å) as a result of the rotation of about one degree of the His286 side chain around the Cβ−Cγ bond toward the alcohol oxygen.

TABLE 4: The Relative Energies of the Key Points of the Studied Reactions[a]

	ΔE/kcal mol^{-1}									
	P1		TS1		IS		TS2		P2	
Rc	**3.7**	(4.5)	**13.5**	(11.2)	**10.7**	(7.4)	**11.9**	(9.7)	**0.0**	(0.0)
Rm	**0.0**	(2.4)	**5.4**	(4.8)	**2.7**	(0.0)	**10.2**	(9.7)	**3.2**	(5.9)
Sc	**0.0**	(0.0)	**14.1**	(11.0)	**8.1**	(3.1)				
Sm	**1.0**	(1.2)	**6.8**	(4.1)	**4.0**	(0.0)	**9.5**	(8.0)	**0.0**	(0.7)

[a] IS is the initial state (the covalent BCL−**1** complex), P1 and P2 are the final states, ester and alcohol, respectively, and TS1 and TS2 are the transition points. In parentheses are given the relative energies of the hydrated BCL−**1** complexes. The energies recalculated with water removed are in bold. For better understanding, see Scheme 2.

After the proton transfer is completed and the covalent bond between a substrate and the protein is broken, the substrate, in the final step, approaches the exit of the BCL binding site with its phenyl ring pointing toward the water. Unfavorable interactions between the nonpolar part of the substrate and the polar water molecules artificially increase the energies of the final structures. To obtain the more realistic energies for the products, we removed the water and recalculated the energy barriers. The reaction diagrams (energy profiles) obtained in this way for **Rc**, **Rm**, and **Sm** are shown in Figure 5.

The recalculated relative energies of the key points in the reaction profiles are given in bold in Table 4. Water is necessary to maintain the stability of the protein, but the facts that BCL activity is the highest at the interface of water and organic phase, and that the enantiomeric ratio was measured in an organic solution, justify the procedure used in this case.

The energy profile for the **Rm** binding mode revealed a lower energy barrier for the covalent binding of the ester (P1) to the enzyme (5.4 kcal mol^{-1}) than for the alcohol (P2) binding to the acyl-enzyme (7.0 kcal mol^{-1}) (Table 5). Formation of the covalent complexes seems to be energetically less demanding in the **Rm** binding mode than in the **Rc** binding mode where the barriers for *R*-**1** and *R*-**E1** binding are 11.9 and 9.8 kcal mol^{-1}, respectively.

The energy barriers for transformation from the initial, covalent complex to the noncovalent BCL−**E1** complex are similar for both enantiomers when they are bound in the orientations determined by molecular modeling, **Rm** and **Sm** (2.7 and 2.8 kcal mol^{-1}, respectively), and they are lower than the barriers for transformation to the noncovalent BCL−**1**

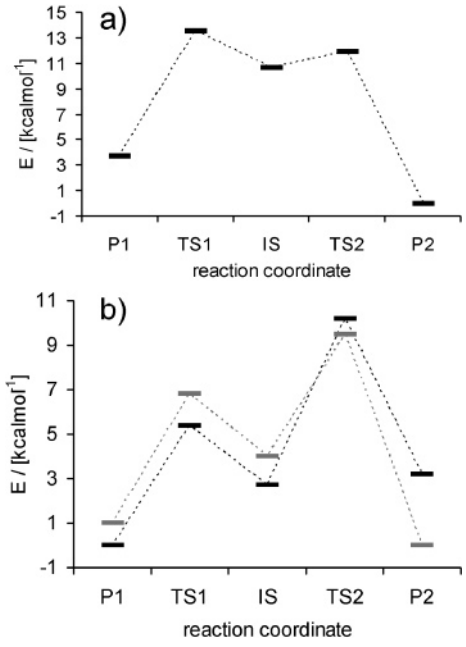

Figure 5. The energy profiles determined for the: (a) **Rc**, (b) **Rm** (black) and **Sm** (gray) binding modes. Only the relative energies between different stages of the reactions (modeled for different complexes) can be compared, but not the energies of the equivalent stages ("points at the reaction curve") for different complexes. See Scheme 2 for a better understanding of the key point names.

TABLE 5: Relative Energies for the Studied Reactions

	energy differences (kcal mol^{-1})			
initial structure	TS1-P1	TS1-IS	TS2-IS	TS2-P2
Rc	9.8	2.8	1.2	11.9
Rm	5.4	2.7	7.5	7.0
Sc	14.1	6.0		
Sm	5.8	2.8	5.5	9.5

complex (7.5 and 5.5 kcal mol^{-1}, respectively). Apparently, the ester formation seems to be slightly easier than hydrolysis in these binding modes. In contrast, hydrolysis, IS→P2 reaction, seems to be more plausible than esterification, IS→P1 reaction, in the **Rc** binding mode; the energy barriers are 1.2 and 2.8 kcal mol^{-1}, respectively (Table 5).

Comparison between the corresponding energies of different complexes is not straightforward. The crystal structures of the BCL complexes 1HQD and 2NW6 differ slightly (rms distance 0.13 Å), as do the structures of the **Rm** and **Sm** complexes. The initial structure for the modeled complexes was 1HQD, but a previous molecular modeling study resulted in slight deviations from the original one. As a result, direct comparison of the energies of different complexes is not possible. However, the major differences are in the orientation of a few side chains on the protein surface, while the shape of the lipase active site is almost identical in all of the complexes. This enables extraction of the substrate from the key points determined on the reaction pathway and its insertion into the **Sc** protein. The new complexes were reoptimized (Supporting Information, Table 1), with the reaction coordinate constrained to the desired value, and after removal of the constraints, the energies were calculated. The results are given in Table 2. However, these results should be taken with caution, especially for the complex immersed in the water, because they are adjusted to **Sc** complex, and in the case of the other complexes they might need some dynamics simulation to adjust.

The tetrahedral intermediates for two enantiomers differ in energy by about 5.5 kcal mol^{-1} (9 kcal mol^{-1} in the absence of water) if the fast-reacting enantiomer binds in the **Rm** and 8.8 kcal mol^{-1} (5.5 kcal mol^{-1} with water absent) if it binds in the **Rc** orientation (Table 2). The E value (defines the lipase enantioselectivity, $E = (k_{cat}/K_M)_{FAST}/(k_{cat}/K_M)_{SLOW}$) determined for the reaction stopped at 50.3% conversion was about 15 000.[19] Such a high lipase enantioselectivity toward **1** can be discussed from both kinetic and thermodynamic points of view. The energy profiles for the *S* and *R* alcohol binding in **Sm** and **Rm** modes, respectively, are similar with about 2.5 kcal mol^{-1} lower barrier for the conversion of the *R* enantiomer than the *S* one. Also, the noncovalent complex between BCL and *R*-alcohol (P2 for the binding mode **Rm**) has about 4.5 kcal mol^{-1} lower energy than the noncovalent complex between BCL and *S*-alcohol (P2 for the binding mode **Sm**). Apparently BCL will preferably bind and chemically transform the *R*-enantiomer of the secondary alcohol rather than the *S* one.

Thermodynamically the high enantioselectivity can be explained according to the hypothesis that the free energy difference of the tetrahedral intermediates for two enantiomers is proportional to the lipase enantioselectivity, $\Delta\Delta G = -RT \ln(E)$. Regarding the experimentally determined value of E (15 000), their energy difference should be about 6 kcal mol^{-1}. The results of the present study agree well with the kinetic resolution measurements (energy difference for the **Sm** and **Rm** TIs is about 5.5 kcal mol^{-1} in water; see Table 2). It should be emphasized, however, that the calculated energy difference corresponds to enthalpy, and not to the binding free energy; that is, the entropic part of ΔG is missing. According to our rough estimates, the desolvation entropy is similar for both enantiomers, and the conformational entropy contribution to the binding free energy increases the enantiomeric ratio approximately by a factor of 2 (see Supporting Information for details). The accurate free energy calculations could also be the subject of further investigations because the B3LYP/6-31G(d)/CHARMM method is not suitable for thermal averaging and free energy calculations. A possible way to determine the free energy difference of the relevant tetrahedral intermediates would be the empirical valence bond method.[40] However, the goal of this work was successfully achieved; it was proved that **Sc** is not a productive binding mode, and the computational results agree well with the experimentally measured enantioselectivity.

The chemical transformation of the slowly reacting enantiomer probably proceeds via formation of the tetrahedral intermediate in which both hydrogen bonds to Nϵ2 of His286 (His286 − alcohol oxygen and His286 − Oγ of Ser87) are formed, that is, with its binding in the **Sm** orientation. According to our QM/MM calculations, the chemical transformation of the substrate bound in the **Sc** orientation is not possible via a tetrahedral intermediate. Therefore, one could speculate that in this case the chemical transformation might occur only via a direct displacement.

Conclusion

Bacterial lipases are interesting for biotechnology because of their high enantioselectivity toward chemically and pharmaceutically important compounds. This Article describes a study of the enantioselectivity of one of the most often used bacterial lipase (the *Burkholderia cepacia* lipase) toward secondary alcohols, the important building blocks for many chiral drugs. The goal of our study was to find out if the experimentally determined binding modes for the phosphonate inhibitor can be considered as productive binding modes for secondary alcohols and their esters. Could the substrate bound in this way be chemically modified? QM/MM calculations showed that **Sc**

is not a productive binding mode. The computational results agree well with the experimentally measured enantioselectivity.

Acknowledgment. This work was supported by grants 098-1191344-2943 and 098-1191344-2860 from the Ministry of Science, Education, and Sport of Croatia and two Bilateral scientific projects between the Republic of Slovenia and the Republic of Croatia: Structure and dynamics of (bio)molecules and Computational Study of Structure and Dynamics of Proteins. We wish to thank Dr. Aleksandar Višnjevac for help with crystallization experiments and Dr. Gregor Gunčar for assistance with data collection and processing.

Supporting Information Available: Table showing the key point relative energies for the studied reactions recalculated with identical (**Sc**) proteins. This material is available free of charge via the Internet at http://pubs.acs.org.

References and Notes

(1) Kazlauskas, R. J.; Bornscheuer, U. T. In *Biotransformations with Lipases in Biotechnology*; Rehm, H. J., Reed, G., Pühler, A., Stadler, P. J. W., Kelly, D. R., Eds.; VCH Publishers: Weinheim, Germany, 1998; Vol. 8, pp 37−191.

(2) Roberts, S. M. *J. Chem. Soc., Perkin Trans.* **2000**, *1*, 1611−633.

(3) Schmid, R. D.; Verger, R. *Angew. Chem., Int. Ed.* **1998**, *37*, 1608−1633.

(4) Faber, K. *Biotransformations in Organic Chemistry*, 3rd ed.; Springer: Berlin, 1997.

(5) Laumen, K.; Schneider, M. P. *J. Chem. Soc., Chem. Commun.* **1988**, 598−600.

(6) Kim, K. K.; Song, H. K.; Shin, D. H.; Hwang, K. Y.; Suh, S. W. *Structure* **1997**, *5*, 173−185.

(7) Schrag, J. D.; Li, Y.; Cygler, M.; Lang, D.; Burgdorf, T.; Hecht, H. J.; Schmid, R.; Schomburg, D.; Rydel, T.; Oliver, J. D.; Strickland, L. C.; Dunaway, C. M.; Larson, S. B.; Day, J.; McPherson, A. *Structure* **1997**, *5*, 187−202.

(8) Lang, D. A.; Mannesse, M. L. M.; De Haas, G. H.; Verheij, H. M.; Dijkstra, B. W. *Eur. J. Biochem.* **1998**, *254*, 333−340.

(9) Lang, D. A.; Dijkstra, B. W. *Chem. Phys. Lipids* **1998**, *93*, 115−122.

(10) Zuegg, J.; Hönig, H.; Schrag, J. D.; Cygler, M. *J. Mol. Catal. B* **1997**, *3*, 83−98.

(11) Haeffner, F.; Norin, T.; Hult, K. *Biophys. J.* **1998**, *74*, 1251−1262.

(12) Schulz, T.; Pleiss, J.; Schmid, R. D. *Protein Sci.* **2000**, *9*, 1053−1062.

(13) Nakamura, K.; Tekenaka, K. *Tetrahedron: Asymmetry* **2002**, *13*, 415−422.

(14) Tomić, S.; Kojić-Prodić, B. *J. Mol. Graphics Modell.* **2002**, *21*, 241−252.

(15) Tomić, S.; Bertoša, B.; Kojić-Prodić, B.; Kolosvary, I. *Tetrahedron: Asymmetry* **2004**, *15*, 1163−1172.

(16) Guieysse, D.; Salagnad, C.; Monsan, P.; Remaud-Simeon, M.; Tran, V. *Tetrahedron: Asymmetry* **2003**, *14*, 1807−1817.

(17) Raza, S.; Fransson, L.; Hult, K. *Protein Sci.* **2001**, *10*, 329−338.

(18) Ljubović, E.; Šunjić, V. *Tetrahedron: Asymmetry* **1997**, *8*, 1−4.

(19) Luić, M.; Tomić, S.; Leščić, I.; Ljubović, E.; Šepac, D.; Šunjić, V.; Vitale, L.; Saenger, W.; Kojić-Prodić, B. *Eur. J. Biochem*. **2001**, *268*, 3964−3973.

(20) Otwinowski, Z.; Minor, W. *Methods Enzymol.* **1997**, *276*, 307−326.

(21) French, G. S.; Wilson, K. S. *Acta Crystallogr., Sect. D: Biol. Crystallogr.* **1978**, *34*, 517−519.

(22) The CCP4 Suite: Programs for Protein Crystallography. *Acta Crystallogr., Sect. D: Biol. Crystallogr.* **1994**, *50*, 760−763.

(23) Brünger, A. T.; Adams, P. D.; Clore, G. M.; DeLano, W. L.; Gros, P.; Grosse-Kunstleve, R. W.; Jiang, J.-S.; Kuszewski, J.; Nilges, M.; Pannu, N. S.; Read, R. J.; Rice, L. M.; Simonson, T.; Warren, G. L. *Acta Crystallogr., Sect. D: Biol. Crystallogr.* **1998**, *54*, 905−921.

(24) Jones, T. A.; Zou, J.-Y.; Cowan, S. W.; Kjeldgaard, M. *Acta Crystallogr., Sect. A: Found. Crystallogr.* **1991**, *47*, 110−119.

(25) Laskowski, R. A.; MacArthur, M. W.; Moss, D. S.; Thornton, J. M. *J. Appl. Crystallogr.* **1993**, *26*, 283−291.

(26) Tomić, S.; Ramek, M. *J. Mol. Catal. B* **2006**, *38*, 139−147.

(27) Brooks, B. R.; Burccoleri, R. E.; Olafson, B. D.; States, D. J.; Karplus, M. *J. Comput. Chem.* **1983**, *4*, 187−217.

(28) MacKerell, A. D., Jr.; Bashford, D.; Bellott, M.; Dunbrack, R. L., Jr.; Evanseck, J. D.; Field, M. J.; Fischer, S.; Gao, J.; Guo, H.; Ha, S.; Joseph-McCarthy, D.; Kuchnir, L.; Kuczera, K.; Lau, F. T. K.; Mattos, C.; Michnick, S.; Ngo, T.; Nguyen, D. T.; Prodhom, B.; Reiher, W. E., III; Roux, B.; Schlenkrich, M.; Smith, J. C.; Stote, R.; Straub, J.; Watanabe, M.; Wiorkiewicz-Kuczera, J.; Yin, D.; Karplus, M. *J. Phys. Chem. B* **1998**, *102*, 3586−3616.

(29) (a) Schmidt M. W.; Baldridge, K. K.; Boatz, J. A.; Elbert, S. T.; Gordon, M. S.; Jensen, J. H.; Kosecki, S.; Matsunaga, N.; Nguyen, K. A.; Su, S. J.; Windus, T. L.; Dupuis, M.; Montgomery, J. A. *J. Comput. Chem.* **1993**, *14*, 1347. (b) Gordon, M. S.; Schmidt, M. W. *Advances in electronic structure theory: GAMESS a decade later*; Elsevier: Amsterdam, 2005; pp 1167−1189 (published online, see: http://www.msg.chem.iastate.edu/gamess/).

(30) Das, D.; Eurenius, K. P.; Billings, E. M.; Sherwood, P.; Chatfield, D. C.; Hodošček, M.; Brooks, B. R. *J. Chem. Phys*. **2002**, *117*, 10534−10547.

(31) Kovach, I. M.; Huhta, D.; Baptist, S. *J. Mol. Struct. (THEOCHEM)* **1991**, *226*, 99−110.

(32) Cahn, R. S.; Ingold, C.; Prelog, V. *Angew. Chem.* **1966**, *78*, 413−447.

(33) Mezzetti, A.; Schrag, J. D.; Cheong, C. S.; Kazlauskas, R. J. *Chem. Biol.* **2005**, *12*, 427−437.

(34) Hanson, K. *Arch. Biochem. Biophys.* **1981**, *211*, 575−588.

(35) Cygler, M.; Grochulski, P.; Kazlauskas, R. J.; Schrag, J. D.; Bouthillier, F.; Rubin, B.; Serreqi, A. N.; Gupta, A. K. *J. Am. Chem. Soc.* **1994**, *116*, 3180−3186.

(36) Derewenda, Z. S.; Derewenda, U.; Kobos, P. M. *J. Mol. Biol.* **1994**, *241*, 83−93.

(37) Cassidy, C. S.; Lin, J.; Frey, P. A. *Biochemistry* **1997**, *36*, 4576−4584.

(38) Kuhn, P.; Knapp, M.; Soltis, S. M.; Ganshaw, G.; Thoene, M.; Bott, R. *Biochemistry* **1998**, *37*, 13446−13452.

(39) Anderson, V. A.; Ruszczycky, M. W.; Harris, M. E. *Chem. Rev.* **2006**, *106*, 3236−3251.

(40) Warshel, A. *Computer Modelling of Chemical Reactions in Enzymes and Solutions*; John Wiley and Sons: New York, 1991.